Alma Mater Studiorum · Università di Bologna

Scuola di Scienze
Dipartimento di Fisica e Astronomia
Corso di Laurea in Fisica

Statistical Analysis of Oceanographic Extreme Events

Relatore:
Dott. Francesco Trotta

Correlatore:
Prof.ssa Nadia Pinardi

Presentata da:
Francesco Maria Benfenati

Anno Accademico 2019/2020

-There's no such thing as bad weather, only bad equipment-
(Scout proverb)

A Giulio, per la sua amicizia e la sua ironia

Abstract

ENGLISH

Extreme environmental sea conditions can have significant impact on navigation safety and/or successful search and rescue operations. Statistical techniques are crucial for accurately quantifying the likelihood of extreme events and monitoring changes in their frequency and intensity. Extreme events "live" in the tail of a probability distribution function (PDF); thus, it is critical to quantify the PDF on the tail, many standard deviations far from the mean.

The significant wave height (SWH) is the parameter generally used to characterize sea states intensity. A valid analysis of extremes in the distribution tail requires long time series for obtaining reasonable estimates of rare events intensity and frequency. However, observational datasets (i.e. historical data from buoys), are often absent and numerical wave hindcasts are used instead. One advantage of using such model outputs is that an extreme value analysis over a large area is possible.

This thesis aims to conduct a preliminary analysis of the spatial variations of SWH extreme values along the Mediterranean Sea. We use hourly SWH data from the Med-MFC model (from CMEMS web portal), a numerical wave hindcast for the whole Mediterranean Sea, performed with wave model WAM Cycle 4.5.4, covering the period 2006-2018, with spatial resolution of 0.042° (≈4km). In particular, we consider 11 years model outputs (from 2007 to 2017), focusing on two regions within the Med-MFC model domain: the Ionian Sea and the Iberian Sea regions.

The SWH PDF is fitted by the 2-parameters Weibull PDF reasonably well during both winter (January) and summer (July), with lacks in the description of distribution peak and tail. In comparison, the 3-parameters Exponentiated Weibull PDF seems to be more appropriate but no method was found to demonstrate its better fitness. Finally, an hazard estimation method is proposed basing on the daily return period of waves higher than a certain threshold value, considered dangerous.

keywords:
significant wave height, Mediterranean Sea, Weibull, Exponentiated Weibull, hazard, wave return period

ITALIAN

Condizioni ambientali estreme del mare possono avere un forte impatto sulla navigazione e/o sul successo di operazioni di salvataggio. Le tecniche statistiche sono cruciali per quantificare la presenza di eventi estremi e monitorarne variazioni di frequenza e intensità. Gli eventi estremi "vivono" nella coda di una funzione distribuzione di probabilità (PDF), per questo è importante studiare la PDF in punti lontani diverse deviazioni standard dalla media.
L'altezza significativa dell'onda (SWH) è il parametro solitamente usato per valutare l'intensità degli stati del mare. L'analisi degli estremi nella coda di una distribuzione richiede lunghe serie temporali per stime ragionevoli della loro intesità e e frequenza. Dati osservativi (i.e. dati storici da boe), sono spesso assenti e vengono invece utilizzate ricostruzioni numeriche delle onde, con il vantaggio che l'analisi di eventi estremi diventa possibile su una vasta area.
Questa tesi vuole condurre un'analisi preliminare delle variazioni spaziali dei valori estremi della SWH nel Mediterraneo. Vengono usati dati orari dal modello del Med-MFC (dal portale del CMEMS), una ricostruzione numerica di onde per il Mediterraneo, che sfrutta il modello "WAM Cycle 4.5.4", coprendo il periodo 2006-2018, con risoluzione spaziale 0.042° (≈ 4km). In particolare, consideriamo dati di 11 anni (dal 2007 al 2017), concentrandoci sulle regioni del Mar Ionio e del Mar Iberico.
La PDF della SWH è seguita piuttosto bene dall'andamento di una curva Weibull a 2 parametri sia durante l'inverno (Gennaio) che durante l'estate (Luglio), con difetti per quanto riguarda il picco e la coda della distribuzione. A confronto, la curva a 3 parametri Weibull Esponenziata sembra essere più appropriata, anche se non è stato trovato un metodo per dimostrare che sia un fit migliore. Alla fine, viene proposto un metodo di stima del rischio basato sul periodo giornaliero di ritorno delle onde più alte di un certo valore di soglia, ritenute pericolose.

parole chiave:
altezza significativa dell'onda, Mar Mediterraneo, Weibull, Weibull Esponenziata, rischio, periodo di ritorno dell'onda

Contents

Chapter 1

Introduction

Extreme environmental sea conditions can have significant impact on navigation safety and/or successful search and rescue operations. Statistical techniques are crucial for accurately quantifying the likelihood of extreme events and monitoring changes in their frequency and intensity.
The first step in reaching this goal is to understand meteo-oceanographic dominant processes. In this attempt, many researches during the last years have analysed the behaviour of probability distribution functions (PDFs) of meteo-oceanographic fields. Sometimes, this is possible by studying the PDF of advected scalar tracers such as chemical concentration or temperature [18]. In fact, extreme events "live" in the tail of a probability distribution function; thus, it is critical to quantify the PDF on the tail, many standard deviations far from the mean.

Among the others, 2-parameters Weibull PDF seems to be appropriate for investigating wind speed [26] and surface currents. Peter C. Chu shows how Weibull PDF is a good fit for surface (0-50 m) tropical Pacific current speeds distribution [10], demonstrating this result can be extended for global oceans [11]. In 2011, Weibull PDF is used by Gildor and Ashkenazy [29] while investigating surface currents distribution in the Gulf of Eilat/Aqaba, suggesting that wind spatial and temporal variability could induce the spatial variability of Weibull parameters obtained by fitting surface current distribution.
As regards extreme events and hazard evaluation, a recent paper by Sepp Neves and Pinardi [27] proposes an hazard mapping approach for coastal oil spill based on a simulation in Algarve coast, Portugal, after demonstrating that also beached ocean tracer concentration distribution fits a Weibull curve.

In this work, we investigate the use of Weibull PDF for fitting wind-forced significant wave height distribution in two Mediterranean regions, as significant wave height is a parameter generally used to characterize sea states intensity. We also suggest a way of hazard mapping related to wave

height.
In Chapter 2, we introduce the modelling system for simulating the dataset used in this study and we show a few examples of wave height time series in both regions.
In Chapter 3, we propose the use of Weibull PDF for fitting significant wave height distribution in comparison with using Exponentiated Weibull, a more general 3-parameters PDF. Besides, we suggest a way of wave hazard mapping basing on the return period of waves higher than a certain threshold.
In Chapter 4, conclusions are reported.

Chapter 2

Significant wave height dataset from CMEMS Web portal

2.1 The Med-MFC wave hindcast

A valid analysis of extremes in the distribution tail requires long time series for obtaining reasonable estimates of rare events intensity and frequency. However, observational datasets (i.e. historical data from buoys), are often absent and numerical wave hindcasts are used instead. One advantage of using such model outputs is that an extreme value analysis over a large area is possible.

In this study, we used the 2D hourly instantaneous field included in the CMEMS multi-year hindcast product MEDSEA_HINDCAST_WAV_006_012 (Fig. 2.1), by the Mediterranean Monitoring and Forecasting Centre (Med-MFC). This is a 13-year wave hindcast for the Mediterranean Sea covering the period from February 2006 to December 2018[1]. The quality of the Med-MFC wave hindcast is assessed by comparison with in-situ and satellite observations. To notice, as described in the Quality Information Document [8] of CMEMS MEDSEA_HINDCAST_WAV_006_012, the wave model best performs in winter, outside enclosed basin and not near the coast.

As regards the modelling system, hourly instantaneous wave parameters are obtained using set-up and configuration of the Q3/2017 version of the Med-waves analysis and forecast system. Parameters are produced at 1/24° horizontal resolution covering the Mediterranean Sea and extending up to -18.125°W into the Atlantic Ocean. Med-waves is based on wave model WAM Cycle 4.5.4 [15], an improved version of WAM Cycle 4 wave model [14] [3]. The land-sea mask map and the bathymetry map of the modelling system are shown in Fig. 2.2.
WAM model is a third generation wave model which explicitly solves the

[1] see *Copernicus Marine Environment Monitoring Service* server **http://marine.copernicus.eu**

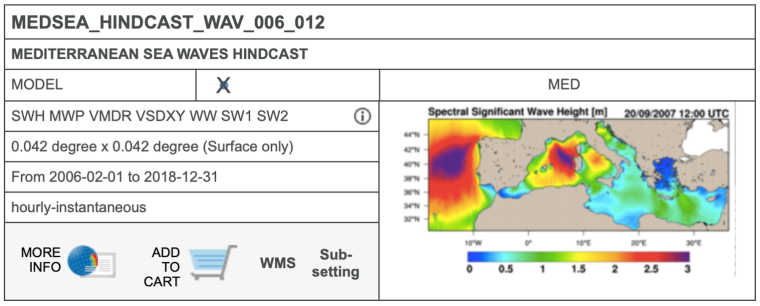

Figure 2.1: Mediterranean wave hindcast product page on CMEMS online server.

basic transport equation describing the evolution of a two dimensional ocean wave spectrum

$$\{\frac{\partial}{\partial t} + \vec{c_g}\frac{\partial}{\partial \vec{x}}\}N(\vec{x}, t, f, \theta) = S_{in} + S_{dis} + S_{NL} + S_{bot}, \tag{2.1}$$

where $\mathrm{N}(\vec{x}, t, f, \theta)$ is the wave energy spectrum, f is the intrinsic angular frequency, θ is the wave direction, $\vec{c_g}$ is the propagation velocity vector (with components in geographical and spectral spaces). Wave transport equation (2.1) is solved without any additional ad hoc assumption on the shape of wave spectrum. Wave source terms include wind input (S_{in}), whitecapping dissipation (S_{dis}), nonlinear transfer (S_{NL}), and bottom friction (S_{bot}). The wind input term is adopted from Snyder during 1981 [7]. The whitecapping dissipation term is based on Hasselmann whitecapping theory [19], while the nonlinear transfer term is a parameterization of the exact nonlinear interactions as proposed during 1985 by Hasselmann and Hasselmann [16] and by Hasselmann et al. [17]. The bottom friction term is based on the empirical JONSWAP model of Hasselmann et al. [2]. The wind input and whitecapping dissipation terms are a further development based on Janssen's quasi-linear theory of wind-wave generation [25][24].

As concerns our data, we studied Significant Wave Height (SWH) parameter, an average quantity obtained throw the model described above, generally used to characterize sea states intensity. We focused on two different regions, one including part of the Ionian Sea, the other part of the Iberian peninsula. In Fig. 2.3, a view of the simulation grid used by the modelling system is shown.

2.2 SWH time series in Ionian Sea and Iberian Sea regions

We considered SWH values in Ionian Sea region, and Iberian Sea region, from 01-01-2007 to 31-12-2017. Hereinafter, we will refer to *Ionian Sea re-*

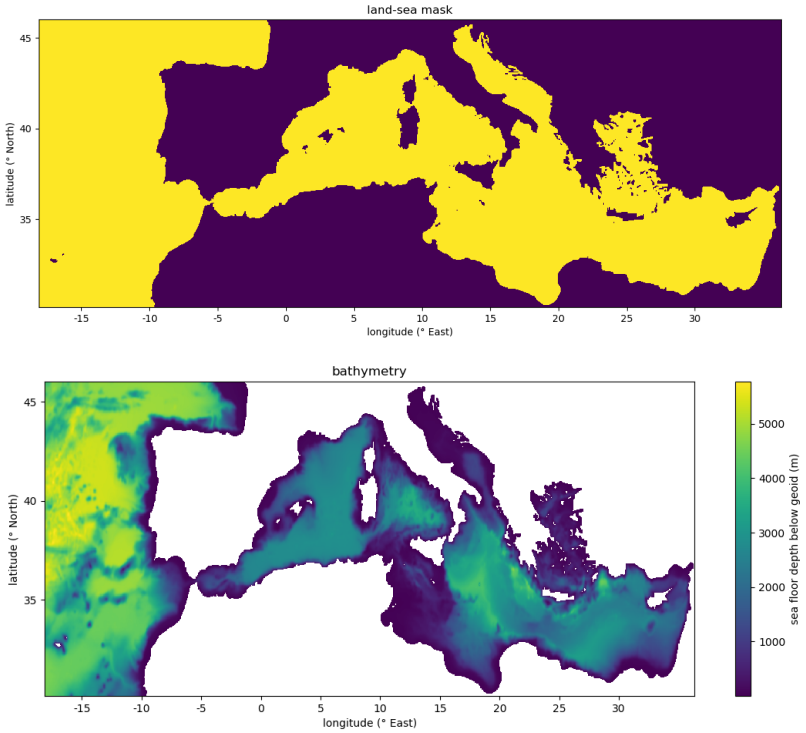

Figure 2.2: Land-sea mask and bathymetry map used by Med-waves in producing wave parameters. Resolution is 1/24°.

gion as the area which goes from 38.48 to 41.19°N latitude, and from 16.42 to 21.00°E longitude. *Iberian Sea region* will be the name of area in latitude range [32.60 ÷ 38.69]°N and longitude range [-9.21 ÷ 0.21]°E. Ionian and Iberian regions respectively consist of 111 longitude x 66 latitude and 227 longitude x 147 latitude simulation points.
Ionian Sea region is part of a semienclosed small area in Mediterranean Sea centre consisting of Adriatic Sea and Ionian Sea. It is divisible in four areas different for their sea quality: the Gulf of Taranto, the Strait of Otranto, the Adriatic Sea area, the open sea area. The Gulf of Taranto is a semienclosed basin in the central-western part of the region, here the modelling system is not trustable very near the coast. The Strait of Otranto is in the region centre, interesting as a sea part bounded on eastern and western sides. Adriatic Sea area is part of southern Adriatic Sea included in our dataset grid. The open sea area is the deepest of Ionian region.
Iberian Sea region is the area around the Strait of Gibraltar, which divides Alboran Sea, the western part of Mediterranean Sea, from North Atlantic Ocean. Here, it is interesting to compare the differences between the Mediterranean and the Oceanic part of the region.

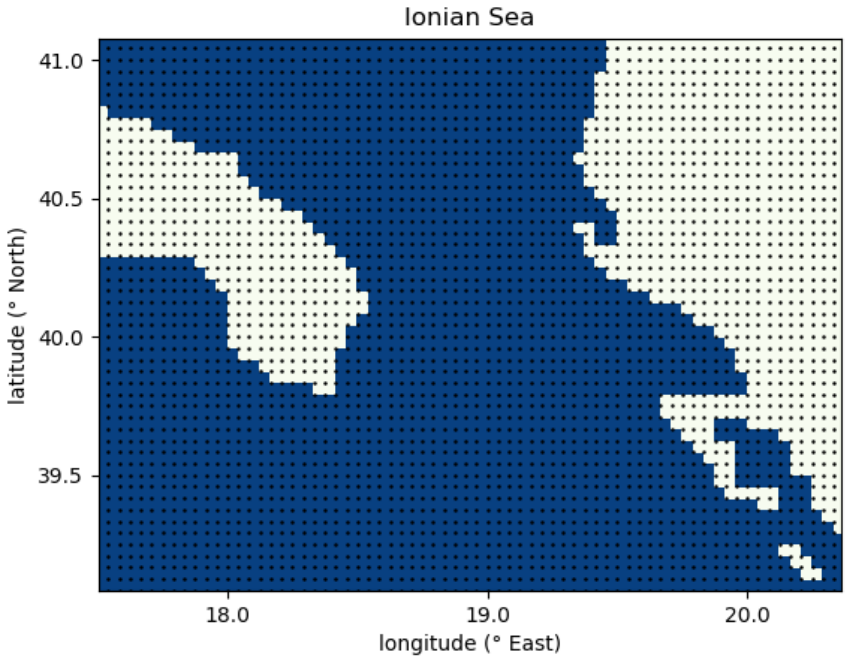

Figure 2.3: View of the spatial grid used by Med-waves in producing wave parameters. Resolution is 1/24°.

Showing few examples of the result of distribution fitting in Chap.3, we will consider SWH distribution in points taken from an arbitrary uniform grid (Fig. 2.4). We will use a 27/24° horizontal step and 20/24° vertical step for Ionian Sea region, a 43/24° horizontal step and 28/24° vertical step for Iberian Sea region. Among these, land points will be excluded and points excessively near to the coast will not be considered, because of the non precise forecast of the modelling system very near the coast. One more point was added within the Gulf of Taranto in the Ionian Sea region, to understand the behaviour of SWH distribution here. Totally, we will show ten different sample points for each region. On the other hand, results reported in Chap. 4 considers all the Med-waves simulation grid points in Fig. 2.2.

In Fig. 2.5, Ionian Sea SWH time series are shown for period 2007-2017 referring to four points from grid in Fig. 2.4, taken from each of the four areas described above. We can notice in 2009 wave height assumes particularly high values in Ionian Sea region. In general, wave height reveals to be greater during winter, with 8 m as maximum value. Open sea waves seem to be the highest, as expected, followed by waves located in the Strait of Otranto. Adriatic Sea waves are the smallest, not overcoming 6 m. Wave height time series suggests this quantity is influenced by seasonality, that's why in next

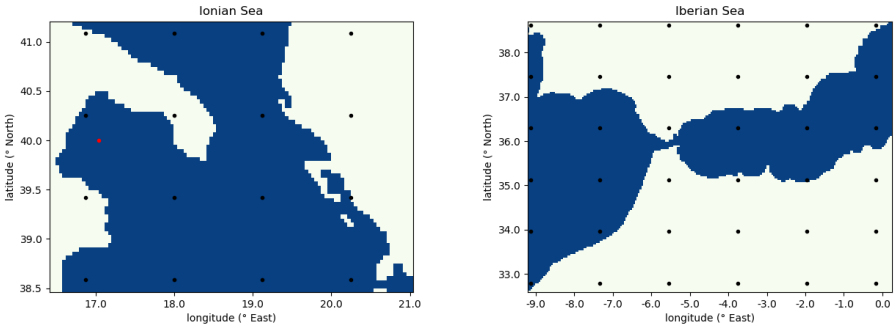

Figure 2.4: sample grids considered in Ionian and Iberian Sea regions. The red point was added to study SWH behaviour within the Gulf of Taranto.

chapter we will also investigate SWH distribution fitting excluding seasonal effects.
The same conclusion about seasonality can be reached for Iberian Sea SWH spectrum (Fig. 2.6). Here, sample points are chosen with the same method as in the Ionian case, taking two Oceanic and two Alboran Sea points. In this area we notice Alboran wave height values are similar to the Ionian region once, while Atlantic waves are higher, reaching near 10 m. In the Mediterranean part, peaks are reached in 2013 and 2015. Differently, in the Oceanic part high values are reached almost every year, with the greatest values in 2008.

In the next chapter, we will study only January and July part of the wave height time series. For our purpose, we believe this comparison sufficiently representative of annual variability, as done by Chu in his 2009 article [11].

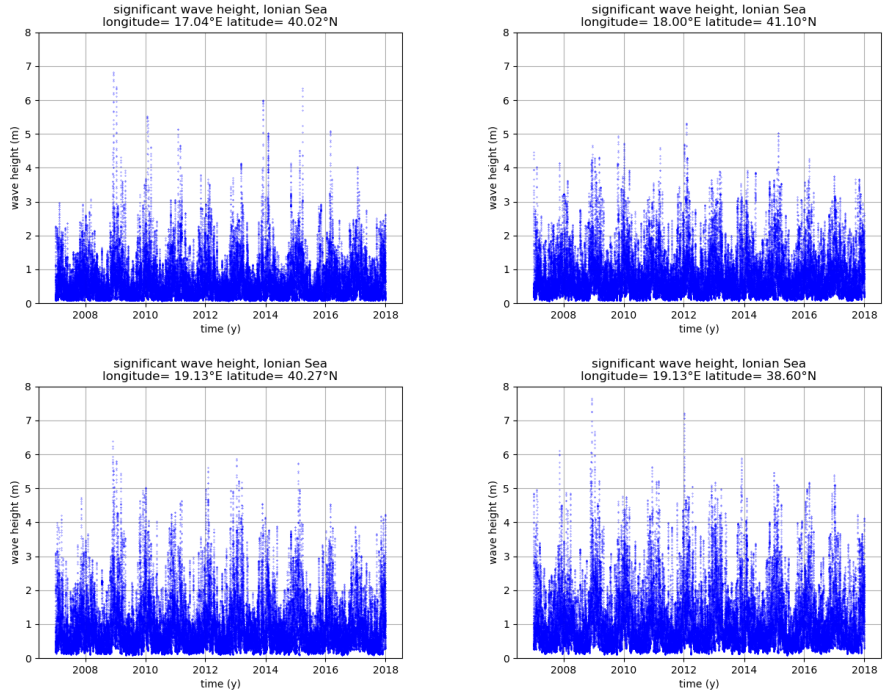

Figure 2.5: SWH values during the period 2007-2017 in four significant points of Ionian Sea region.

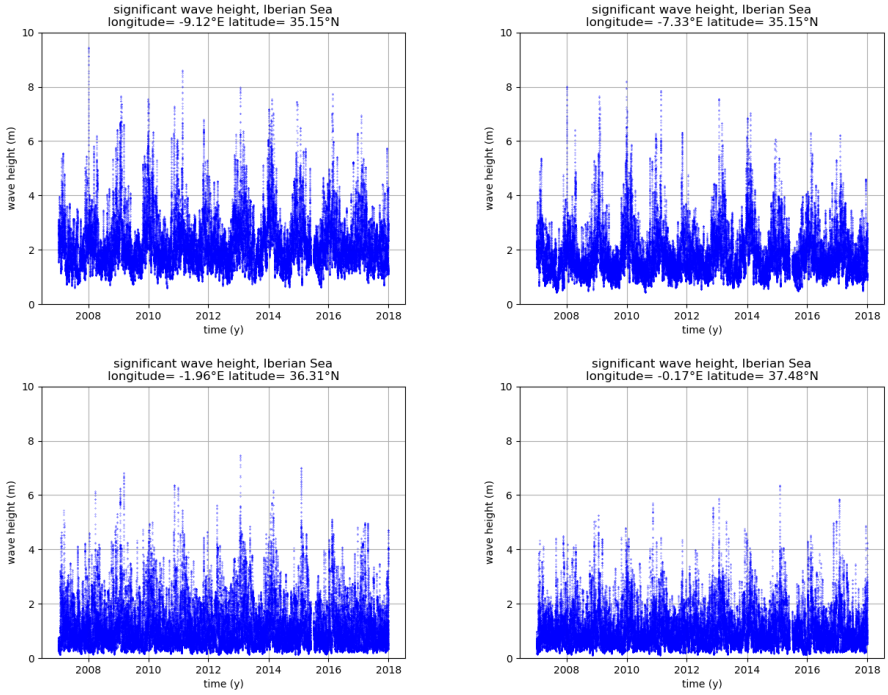

Figure 2.6: SWH values during the period 2007-2017 in four significant points of Iberian Sea region.

Chapter 3

SWH distribution fitting

3.1 Weibull and Exponentiated Weibull distributions

Two different statistical distributions have been used to fit our SWH model datasets: the 2-parameters Weibull (W) distribution and the more general 3-parameters Exponentiated Weibull (EW) distribution, which is a generalization of the Weibull one. This section provides a general background for both of these distributions.
The Weibull distribution is frequently used to model survival, reliability, wind speed, and other data. One reason for this is its flexibility; it can mimic various distributions like the exponential or normal one. The 2-parameters Weibull depends on a shape parameter k and a scale parameter λ [9], with density (PDF), cumulative (CDF) and tail (TF) functions:

$$f_W(x;k,\lambda) = \frac{k}{\lambda}(\frac{x}{\lambda})^{k-1}\exp^{-(\frac{x}{\lambda})^k} \qquad (PDF), \tag{3.1}$$

$$F_W(x;k,\lambda) = 1-\exp^{-(\frac{x}{\lambda})^k} \qquad (CDF), \tag{3.2}$$

$$S_W(x;k,\lambda) = \exp^{-(\frac{x}{\lambda})^k} \qquad (TF). \tag{3.3}$$

EW curve depends on two shape parameter α, k and one scale parameter λ, as described by Pal et al. in 2006 [20]. Its density, cumulative and tail functions are:

$$f_{EW}(x;k,\lambda) = \alpha\frac{k}{\lambda}(\frac{x}{\lambda})^{k-1}\exp^{-(\frac{x}{\lambda})^k}(1-\exp^{-(\frac{x}{\lambda})^k})^{\alpha-1} \qquad (PDF), \tag{3.4}$$

$$F_{EW}(x;k,\lambda) = (1-\exp^{-(\frac{x}{\lambda})^k})^{\alpha} \qquad (CDF), \tag{3.5}$$

$$S_{EW}(x;k,\lambda) = 1-(1-\exp^{-(\frac{x}{\lambda})^k})^{\alpha} \qquad (TF). \tag{3.6}$$

If $\alpha = 1$, EW functions reduces to W ones.
In distribution fitting, the location parameter is set 0 for both theoretical distributions, as appears in the whole upper equation set.

The cumulative distribution function F(x) is obtained integrating the probability density function f(x) in range [0,x], while the tail function S(x), also called *survival function*, is obtained subtracting F(x) to 1:

$$F(x) = \int_0^x f(x')\,dx'; \qquad S(x) = 1 - F(x). \tag{3.7}$$

Tail function is very important in studying extreme events and hazard evaluating, in fact, the larger S(x) is, the more events are contained in distribution tail.

3.2 Distribution fitting

In this Section distribution fitting method and results are shown. For both regions, examples are related to the points considered in Section 2.2 for their locational differences.

3.2.1 The maximum likelihood estimation method

In fitting procedure, W and EW parameters were estimated by using the *maximum likelihood estimation* method. We employed Python3.7 module *scipy.stats* containing a large number of probability distributions as well as library of statistical functions. In particular, we used *scipy.stats.exponweib.pdf* and *scipy.stats.exponweib.fit* methods, where *exponweib* is an implemented continuous random variable class based on (3.4). The first method generates the PDF while the second one produces fitting parameters[1], coherently with Johnson's work *Continuous Univariate Distributions, Vol.s 1,2* [22] [23].

First of all, be $f(x;\vec{\theta})$ PDF of a random variable x, with $\vec{\theta}$=(α,k,λ) EW parameters vector (reducible to W parameters vector in case α=1). The joint PDF for a random vector $\vec{x}$=$\{x_i\}$, collection of N independent samples from $f(x;\vec{\theta})$, is:

$$f(\vec{x};\vec{\theta}) = \prod_{i=1}^{N} f(x_i,\vec{\theta}). \tag{3.8}$$

The maximum likelihood estimate of $\vec{\theta}$ are the parameters which maximize (3.8) for $\vec{x}$ fixed, given by:

$$\vec{\theta}_{est} = arg\max_{\vec{\theta}} f(\vec{x};\vec{\theta}) = arg\min_{\vec{\theta}} l_x(\vec{\theta}), \tag{3.9}$$

where

$$l_x = -\sum_{i=1}^{N} \log f(x_i,\vec{\theta}) = -N\overline{\log f(x_i,\vec{\theta})} \tag{3.10}$$

[1] see online reference on page:
https://docs.scipy.org/doc/scipy/reference/tutorial/stats/continuous.html

(*log* is the natural logarithm). In (3.10), for mean value we use the standard notation

$$\overline{y(\vec{x})} = \frac{1}{N}\sum_{x=1}^{N} y(x_i).$$

3.2.2 Results

At a first glance, distribution fitting results are quite satisfactory. In Fig.s 3.1,3.2, 3.3 and 3.4 distribution fitting graphs are shown for both region in January and July. The four significant sample points are the same as in Fig. 2.5, 2.6. Histogram bins width is 0.1 m.
SWH distribution is fat tailed, especially in January and far from the coast in the open sea area in Ionian Sea region (Fig. 3.1 down right), and in the open ocean area in Iberian Sea region (Fig. 3.3 upper left). In July, when waves are lower, the distribution peak is higher and shifted to the lowest SWH values. Besides, Oceanic points in Iberian Sea region (Fig.s 3.3 and 3.4 upper graphs), present a more Gaussian-shaped distribution, with high SWH minimum values.
On one hand, W PDF seems to be a good fit for SWH distribution, even if not completely satisfying. On the other hand, EW PDF seems best descriptive of distribution peak and - most important in studying extreme events - tail. The first difference about peaks is evident in July, when waves are lower and the distribution peak is greater (Fig.s 3.2, 3.4). The tail fit difference is most visible in January, when wave height is greater, using a semi-logarithmic plot (Fig.s 3.1, 3.3). Furthermore, EW curve better fits the global distribution shape, in particular when SWH minimum values are far from zero in the Oceanic area of Iberian Sea region (Fig.s 3.3, 3.4 upper graphs).

For having an idea of fit shape in each point of the region, W fit parameters are mapped in Fig.s 3.5 and 3.6.
In Ionian Sea region, W scale parameter goes from 0 to 1.8 m in January and from 0 to 0.9 m in July. Higher λ values are in the open sea area and near the Strait of Otranto, which means here the distribution tail is fatter. The shape parameter never goes under 1 and is similarly mapped during both months, with little increasing k values in July, especially near the Strait of Otranto. Greatest k values are in the open sea area and near the south eastern coast. In Iberian Sea region, both parameters are really variable comparing the Alboran Sea and the Oceanic area. In the Mediterranean part, λ and k values are slightly larger than the open sea values in the Ionian case, except for July case of λ whose values are visibly greater. Oceanic fit parameters are significantly higher going to the open ocean, where waves are higher and minimum SHW values are shifted to the right. This is coherent with the more Gaussian shape of SWH distribution discussed before. As in the Ionian case, λ values are larger in winter while k values in summer.

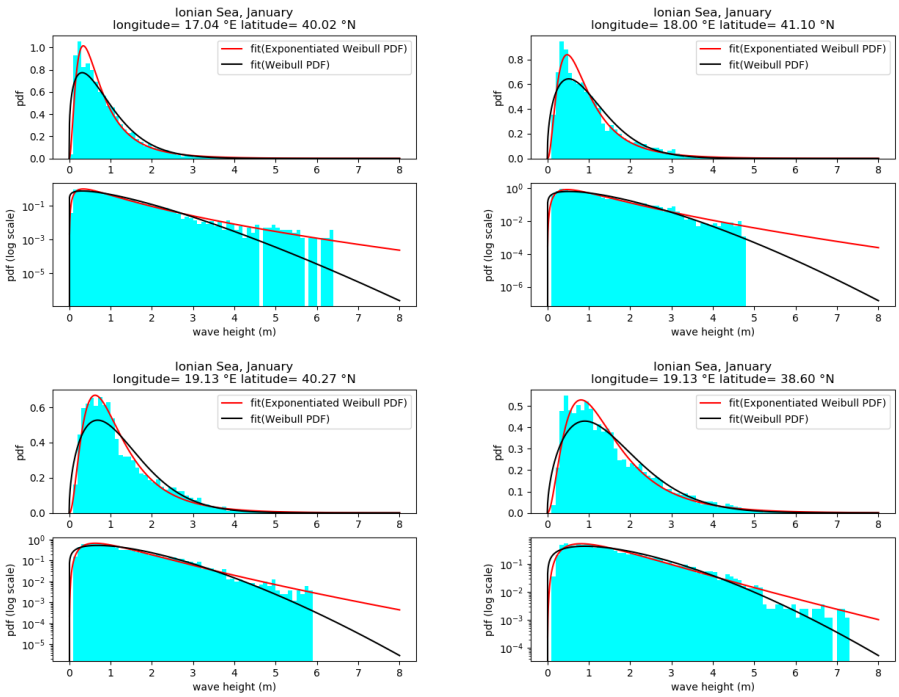

Figure 3.1: SWH distribution fitting during period 2007-2017 in January in four significant points of Ionian Sea region.

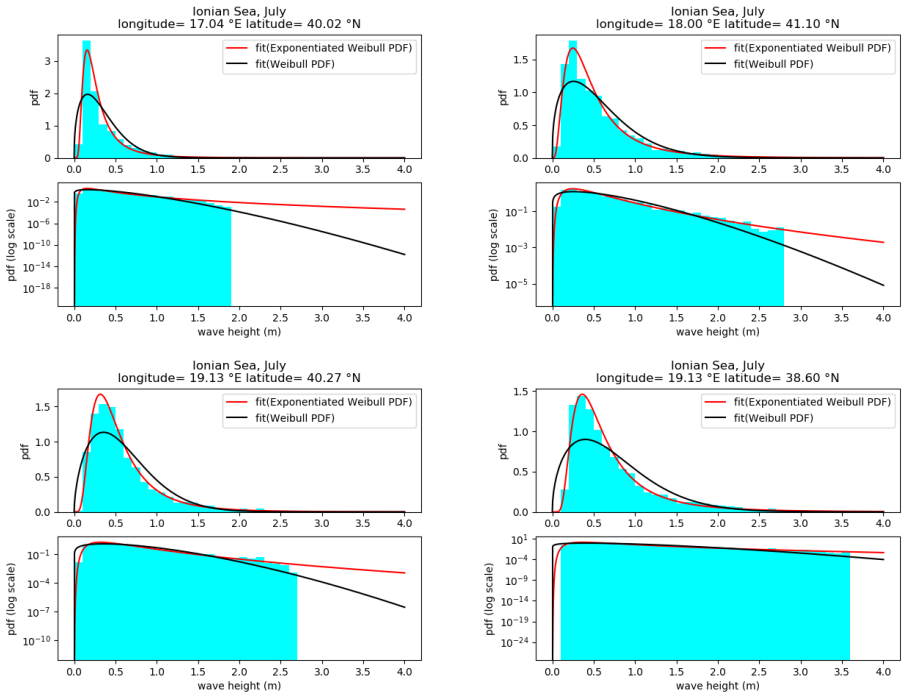

Figure 3.2: SWH distribution fitting during period 2007-2017 in July in four significant points of Ionian Sea region.

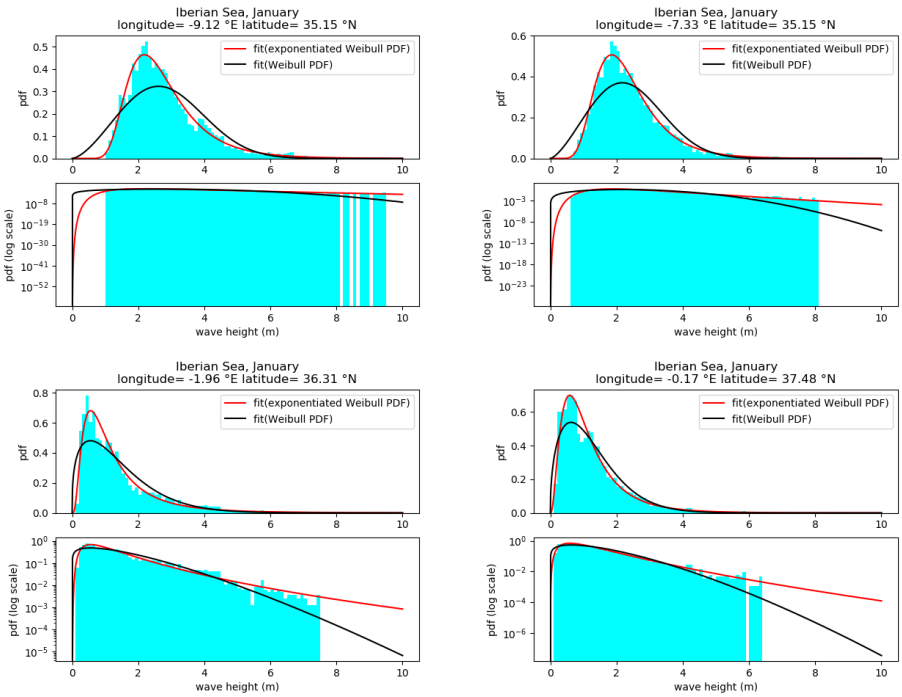

Figure 3.3: SWH distribution fitting during period 2007-2017 in January in four significant points of Iberian Sea region.

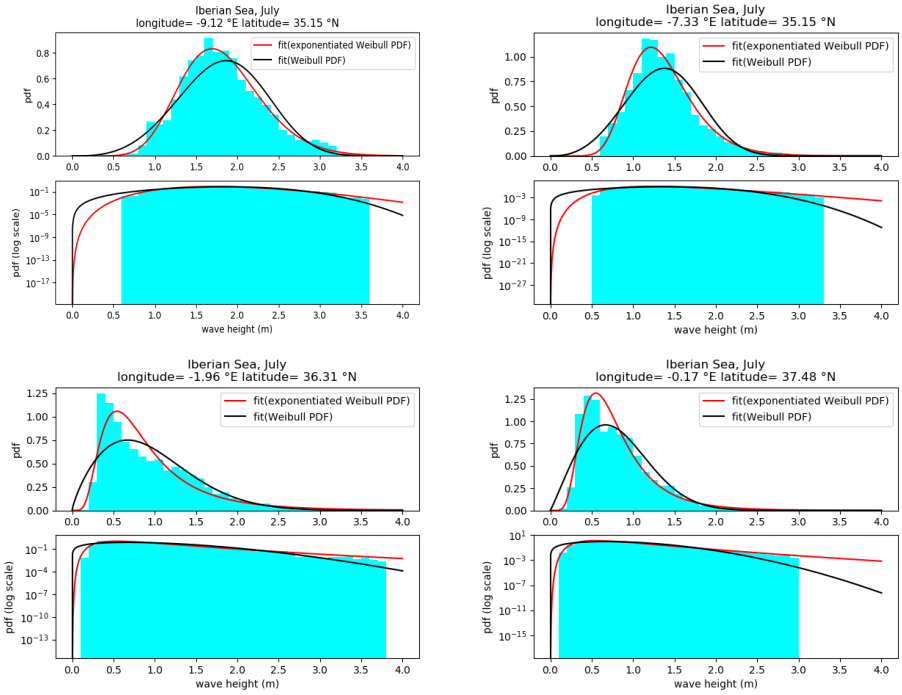

Figure 3.4: SWH distribution fitting during period 2007-2017 in July in four significant points of Iberian Sea region.

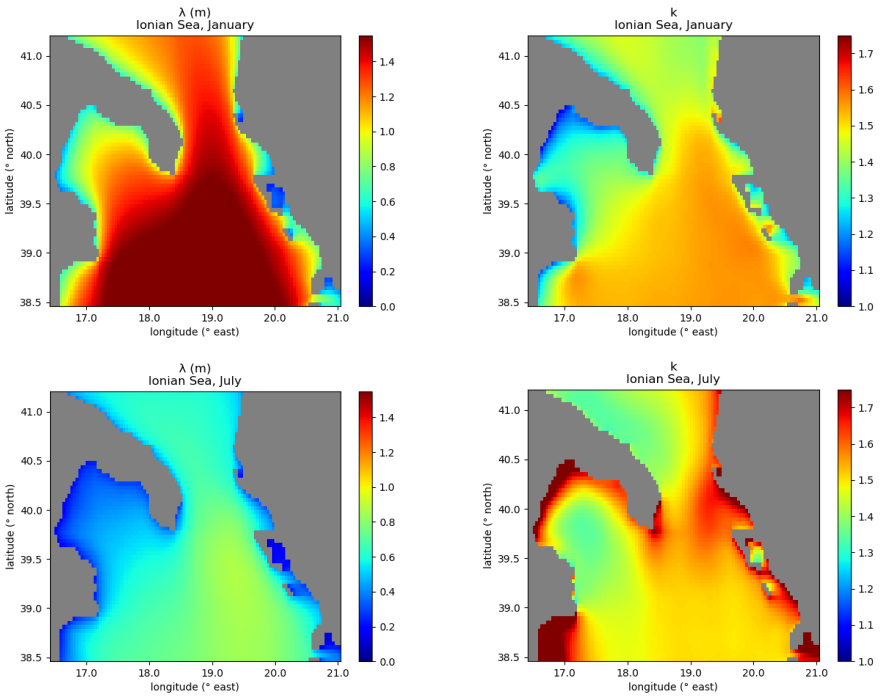

Figure 3.5: Theoretical Weibull scale and shape parameter of January and July fit in Ionian Sea region.

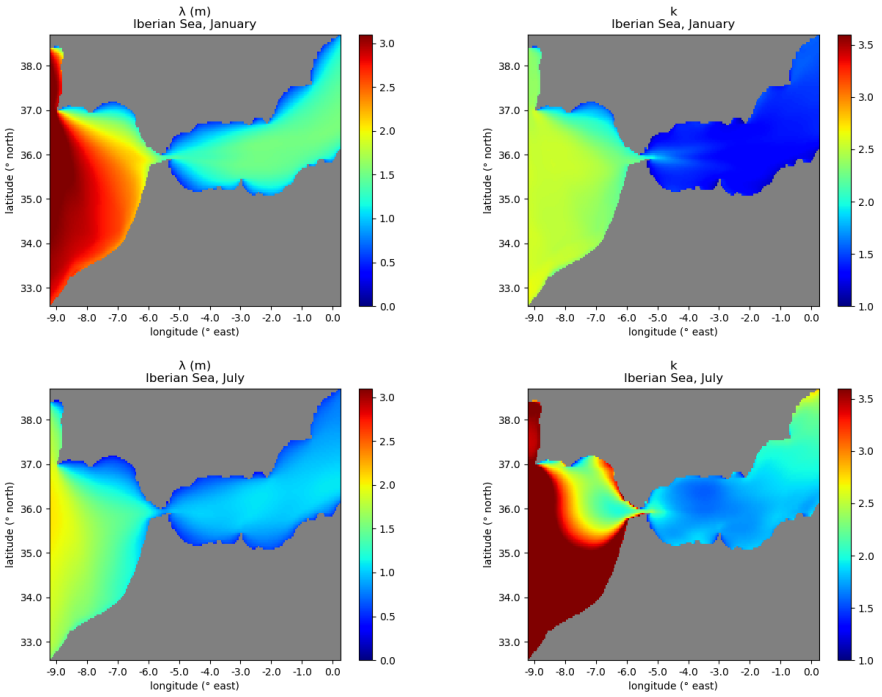

Figure 3.6: Theoretical Weibull scale and shape parameter of January and July fit in Iberian Sea region.

EW fit parameters are shown in Tab.s 3.1 and 3.2 for the ten points from each uniform sample grid considered in Fig. 2.4.
In Ionian Sea region, as for the W case, λ values are lower in summer than in winter. During July, the shape parameter k decreases, unlikely the W case, while the shape parameter α is the one increasing. We notice where α is higher, k is lower. Largest λ values are offshore during winter and near the Strait of Otranto during summer, with great difference between the two seasons. The same seasonal difference is visible for α.
In Iberian Sea region, during July α values increase in the Mediterranean area and decrease in the Oceanic area, with one exception near the coast. In general, shape parameter k is higher in July, with exceptions near the coast.

IONIAN SEA

		January			July		
long. (°E)	lat. (°N)	α	k	λ (m)	α	k	λ (m)
16.88	38.60	25.33	0.47	0.054	110.98	0.41	0.0074
17.04	40.02	6.93	0.58	0.15	410.03	0.28	0.00029
18.00	38.60	5.46	0.72	0.44	316.70	0.30	0.0011
18.00	39.44	4.02	0.77	0.48	311.95	0.29	0.00073
18.00	41.10	6.48	0.64	0.22	18.40	0.46	0.032
19.13	38.60	4.11	0.81	0.60	196.66	0.32	0.0023
19.13	39.44	3.40	0.87	0.65	19.05	0.51	0.056
19.13	40.27	5.18	0.72	0.37	30.31	0.48	0.029
19.13	41.10	5.82	0.64	0.25	73.13	0.38	0.0065
20.25	38.60	3.94	0.82	0.51	228.57	0.32	0.0022

Table 3.1: Theoretical Exponentiated Weibull parameters of January and July fit in ten points from the Ionian Sea region sample grid.

IBERIAN SEA

		January			July		
long. (°E)	lat. (°N)	α	k	λ (m)	α	k	λ (m)
-9.13	33.98	56.97	0.70	0.30	5.66	1.94	1.12
-9.13	35.15	61.75	0.69	0.29	4.76	1.95	1.25
-9.13	36.31	48.81	0.71	0.35	5.18	1.87	1.22
-9.13	37.48	16.40	0.85	0.66	4.48	1.75	1.05
-7.33	35.15	20.72	0.84	0.51	11.47	1.37	0.62
-7.33	36.31	17.63	0.84	0.43	319.35	0.51	0.029
-3.75	36.31	4.84	0.68	0.30	14.28	0.54	0.084
-1.96	36.31	15.56	0.46	0.085	26.72	0.52	0.065
-0.17	36.31	13.04	0.49	0.11	23.30	0.57	0.086
-0.17	37.48	6.23	0.66	0.29	21.93	0.66	0.11

Table 3.2: Theoretical Exponentiated Weibull parameters of January and July fit in ten points from the Iberian Sea region sample grid.

During summer, the scale parameter λ is larger in open ocean points but smaller near the coast and in the Mediterranean part in comparison to the winter month.

3.3 Parameters of W and EW distributions

Four distribution parameters reveal to be important in confirming distribution fitness: mean μ, standard deviation (std) σ, skewness γ_1 and kurtosis γ_2. In Appendix A, we demonstrate how to obtain the four parameters of W and EW distributions, coherently with Chu [10][11] and Pal [20], beginning by their PDFs.
For Weibull PDF, the four parameters become:

$$\mu_{\mathrm{W}} = \lambda\Gamma\Big(1+\frac{1}{k}\Big) \quad , \tag{3.11}$$

$$\sigma_{\mathrm{W}} = \lambda\Big\{\Gamma\Big(1+\frac{2}{k}\Big) - \Gamma^2\Big(1+\frac{1}{k}\Big)\Big\}^{1/2} \quad , \tag{3.12}$$

$$\gamma_{1\mathrm{W}} = \frac{\Gamma\Big(1+\frac{3}{k}\Big) - 3\Gamma\Big(1+\frac{1}{k}\Big)\Gamma\Big(1+\frac{2}{k}\Big) + 2\Gamma^3\Big(1+\frac{1}{k}\Big)}{\Big[\Gamma\Big(1+\frac{2}{k}\Big) - \Gamma^2\Big(1+\frac{1}{k}\Big)\Big]^{\frac{3}{2}}} \quad , \tag{3.13}$$

$$\gamma_{2\mathrm{W}} = \frac{\Gamma\Big(1+\frac{4}{k}\Big) - 4\Gamma\Big(1+\frac{1}{k}\Big)\Gamma\Big(1+\frac{3}{k}\Big) + 6\Gamma^2\Big(1+\frac{1}{k}\Big)\Gamma\Big(1+\frac{2}{k}\Big) - 3\Gamma^4\Big(1+\frac{1}{k}\Big)}{\Big[\Gamma\Big(1+\frac{2}{k}\Big) - \Gamma^2\Big(1+\frac{1}{k}\Big)\Big]^{2}} \quad , \tag{3.14}$$

where Γ is the gamma function.
For EW PDF, we obtain:

$$\mu_{\mathrm{EW}} = \lambda\Gamma\Big(1+\frac{1}{k}\Big)K(\alpha,k) \quad , \tag{3.15}$$

$$\sigma_{\mathrm{EW}} = \lambda\left[\left(\Gamma\Big(1+\frac{2}{k}\Big) - \Gamma^2\Big(1+\frac{1}{k}\Big)K(\alpha,k)\right)K(\alpha,k)\right]^{\frac{1}{2}} \quad , \tag{3.16}$$

$$\gamma_{1\mathrm{EW}} = \frac{\Gamma\Big(1+\frac{3}{k}\Big) - 3\Gamma\Big(1+\frac{1}{k}\Big)\Gamma\Big(1+\frac{2}{k}\Big)K(\alpha,k) + 2\Gamma^3\Big(1+\frac{1}{k}\Big)K^2(\alpha,k)}{\Big[\Gamma\Big(1+\frac{2}{k}\Big) - \Gamma^2\Big(1+\frac{1}{k}\Big)K(\alpha,k)\Big]^{\frac{3}{2}}K^{\frac{1}{2}}(\alpha,k)} \quad , \tag{3.17}$$

$$\gamma_{2\mathrm{EW}} = \frac{\begin{array}{r}\Gamma\Big(1+\frac{4}{k}\Big)-4\Gamma\Big(1+\frac{1}{k}\Big)\Gamma\Big(1+\frac{3}{k}\Big)K(\alpha,k)+\\ +6\Gamma^2\Big(1+\frac{1}{k}\Big)\Gamma\Big(1+\frac{2}{k}\Big)K^2(\alpha,k)-3\Gamma^4\Big(1+\frac{1}{k}\Big)K^3(\alpha,k)\end{array}}{\Big[\Gamma\Big(1+\frac{2}{k}\Big)-\Gamma^2\Big(1+\frac{1}{k}\Big)K(\alpha,k)\Big]^2 K(\alpha,k)} \quad , \tag{3.18}$$

where Γ is the gamma function and:

$$K(\alpha,k) = \sum_{i=0}^{\infty} \frac{(-1)^i}{(i+1)^{-(1+\frac{1}{k})}} P_{\alpha-i}$$
$$\Big(P_{\alpha-i} = \alpha(\alpha-1)(\alpha-2)\cdots(\alpha-i)\Big).$$

As it appears, skewness and kurtosis only depend on shape parameters (k for W PDF and α, k for EW PDF) like the ratio $\frac{\mu}{\sigma}$. This is why the relationships between kurtosis and skewness and between skewness and mean/std may be used to identify the fitness of W and EW distributions for *swh*-PDF from model output.

3.3.1 Comparison between theoretical W PDF and *swh*-PDF parameters

For a data distribution from model output, the four parameters (mean, standard deviation, skewness, kurtosis), are defined as:

$$mean(h) = \frac{1}{N}\sum_{i=1}^{N} h_i \qquad (mean) \tag{3.19}$$

$$std(h) = \sqrt{mean\Big\{[h-mean(h)]^2\Big\}} \qquad (standard\ deviation) \tag{3.20}$$

$$skew(h) = \frac{mean\Big\{[h-mean(h)]^3\Big\}}{std^3(h)} \qquad (skewness) \tag{3.21}$$

$$kurt(h) = \frac{mean\Big\{[h-mean(h)]^4\Big\}}{std^4(h)} - 3 \qquad (kurtosis) \tag{3.22}$$

To calculate mean, standard deviation, skewness and kurtosis we used Python3.7 modules *scipy.stats*, *numpy*. In particular, we employed the following methods: *numpy.mean*, *numpy.std*, *stats.skew* and *stats.kurtosis*, which respectively implement the upper equations (3.19), (3.20), (3.21), (3.22).

In comparing the four theoretical and observational parameters, we use a kurt(skew) and a skew(mean/std) graph to identify Weibull distribution fitness (Fig. 3.7), as done by Chu [10][11]. The relationship between skew(h) and kurt(h) in observations is similar to that for a W variable, with similar

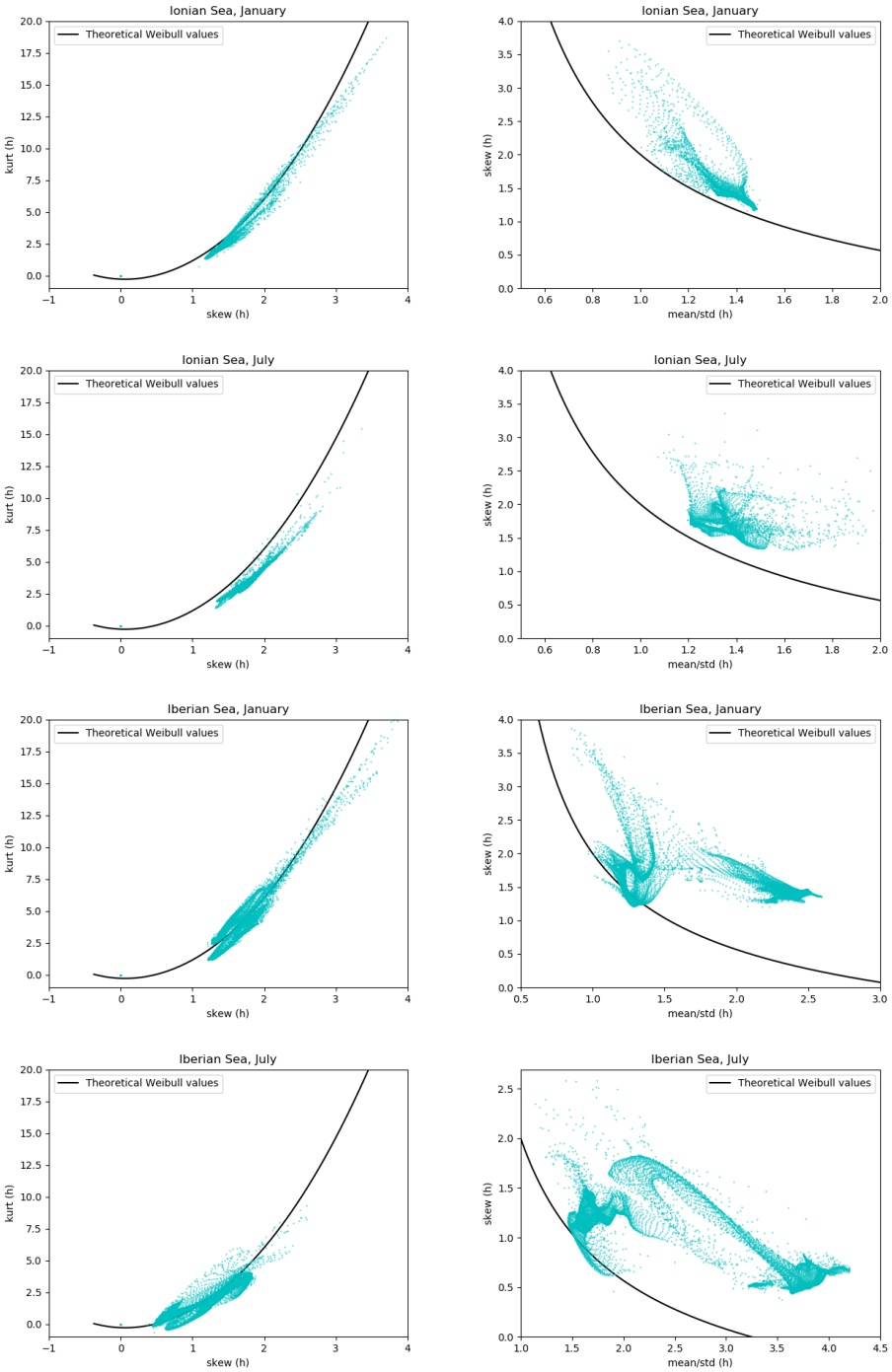

Figure 3.7: Relationship between kurt(h) and skew(h) (left), and between the ratio mean(h)/std(h) and skew(h) (right), for the observational swh-PDFs (dots) and the Weibull distribution (solid curve) in Ionian Sea region and Iberian Sea region during January and July.

features in January and in July for each region. The same can not be said for observational skew(h) in function of ratio mean(h)/std(h), which assumes very particular features, including values both near and far the theoretical W once, really satisfactory only in Ionian Sea during January (Fig. 3.7, the first from the upper right). This seems to be a clue of the good but not excellent fitness of W curve for our observational dataset, suggesting EW curve could be more appropriate.

We tried to demonstrate the best fitness of EW curve with no success. Implementing Eq.s (3.15), (3.16), (3.17), (3.18) and trying to plot the kurt(skew) and the skew(mean/std) graphs for an EW variable, we could not obtain a theoretical continuous function as the one for a Weibull variable. Due to the fact EW relationship between kurt and skew and between skew and mean/std depend on the two shape parameters, not only one, the dataset used in this study may be not large enough for applying this moments-comparing method with sufficient accuracy. Hopefully, future studies could investigate the best fitness of EW PDF for a SWH distribution, using this very method but a much larger dataset or a different ad hoc method.

3.4 Distribution fitting excluding seasonal effects

As seen in Section 2.2, SWH time series seem affected by seasonality. For this reason, SWH distributions have been fitted excluding seasonal effects, too (Fig.s 3.8 and 3.9). The wave height seasonal part has been cut off subtracting to each value of the i-th day (within a month), the eleven-years mean of the averages obtained each year for that day. In particular, a general SWH value simulated as described in Chap. 2, depending on an hourly index i, a daily index j and an annual index k, becomes:

$$h'_{i,j,k} = h_{i,j,k} - \frac{1}{11}\sum_{k'=1}^{11}\left\{\frac{1}{24}\sum_{i'=1}^{24} h_{i',j,k'}\right\}, \tag{3.23}$$

where $h_{i,j,k}$ is the starting SWH value. Negative wave height values resulting from (3.23) have not been considered in distribution fitting.
As it is visible in Fig.s 3.8 and 3.9, the distribution shape becomes very different respect to what seen in Section 3.3.2, when excluding seasonality. The peak is always in correspondence to 0 and the shape is generally more exponential, with thinner tail. W PDF seems well descriptive of the observational distribution shape, with better fitness than EW PDF in almost all the region except for points near the coast and in enclosed basins such as the Gulf of Taranto. The difference between the two theoretical PDFs is excluding seasonality almost perceptible and never as important as seen in Section 3.2.2, in fact, the two distributions tend to be coincident. Results confirm our use of W PDF as fit of SWH distribution.

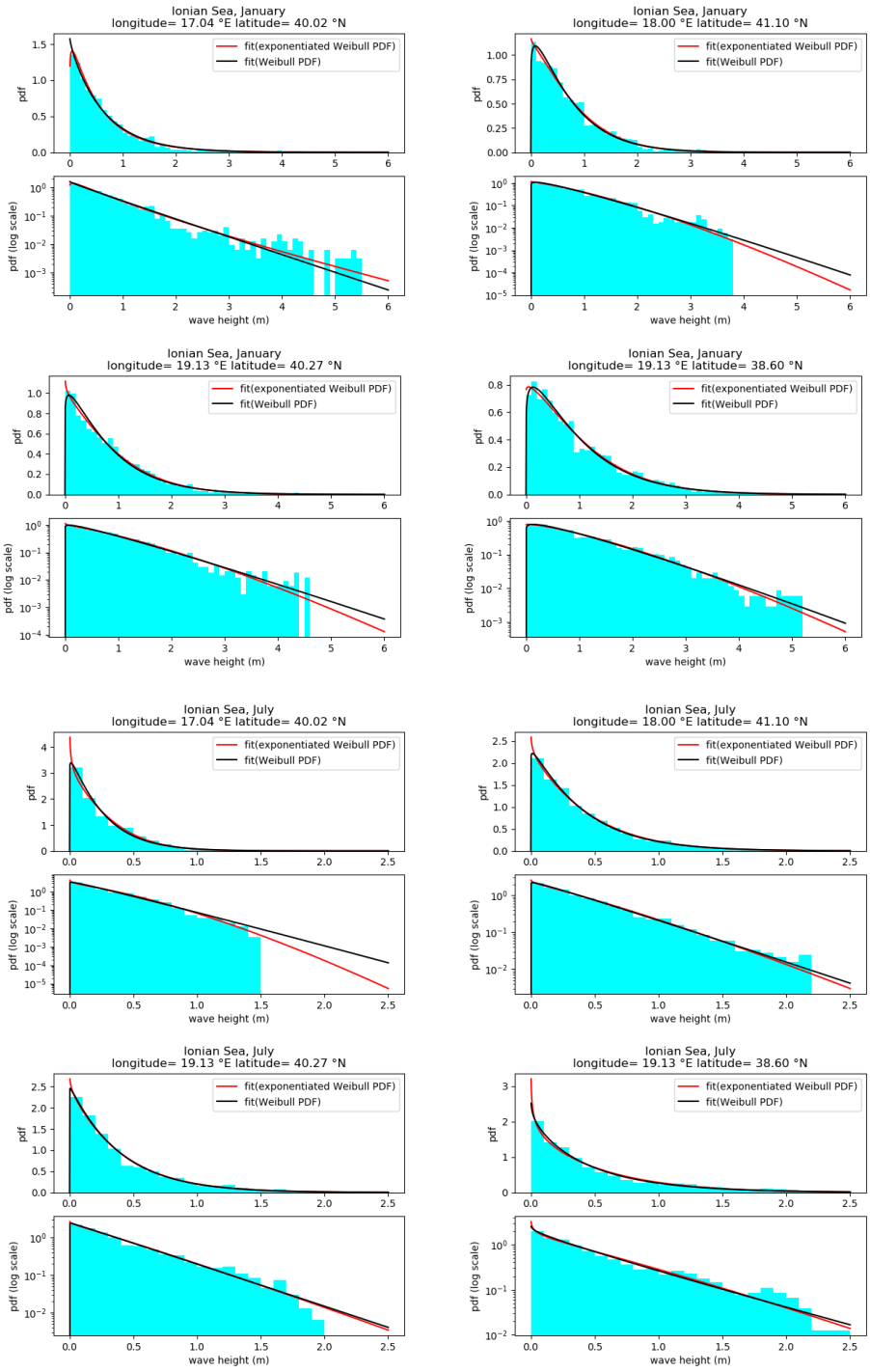

Figure 3.8: Fitting of SWH distribution excluding height part due to seasonality during period 2007-2017 in January and July in four significant points of Ionian Sea region.

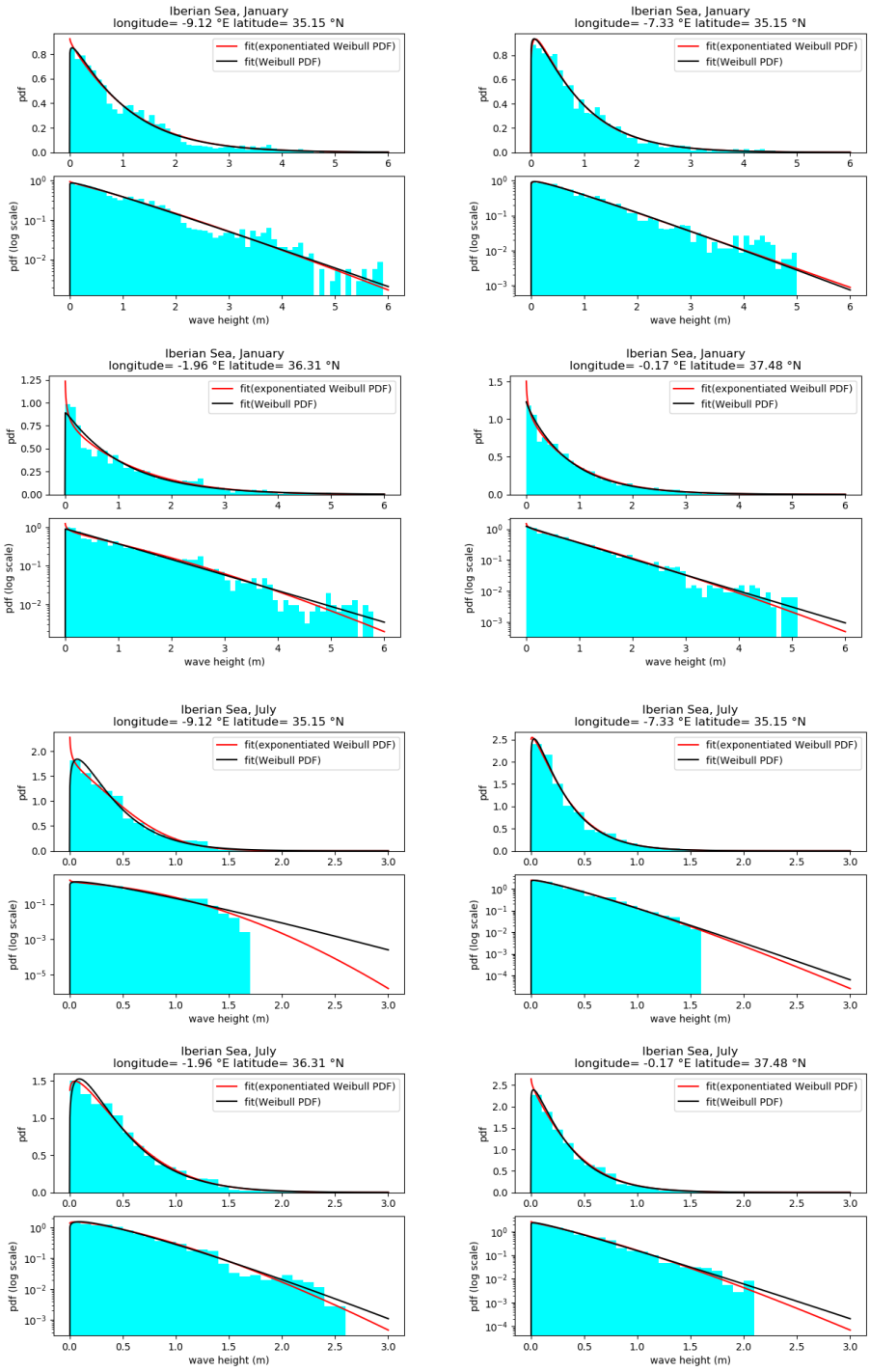

Figure 3.9: Fitting of SWH distribution excluding height part due to seasonality during period 2007-2017 in January and July in four significant points of Iberian Sea region.

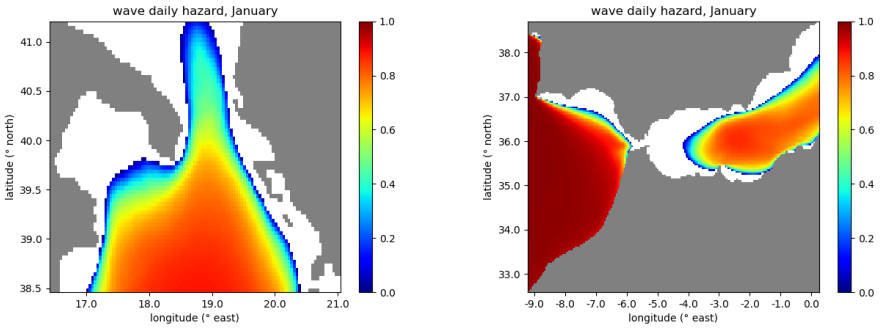

Figure 3.10: Wave daily hazard map in Ionian (left) and Iberian (right) Sea region in January, based on high waves return period with 3 m height as threshold.

3.5 Wave hazard mapping

Once demonstrated in our regions Weibull curve is a good fit for *swh*-PDF, we can look for a method to associate an hazard value to each sea point. This can be a really useful application for maritime routes and rescue operations. Firstly, a way of hazard evaluation must be found. Aware that what makes waves dangerous for boats is the possibility to break against them, this evaluation method would be too long and complicated to be faced in this work. Here, we suggest to base the risk estimation on the daily return period of waves higher than a certain threshold value h_t, which may be reputed dangerous for men overboard. The return period R is, by definition, the average duration of time during which extreme events exceeding a threshold value would occur once [13]:

$$R(h > h_t) = \frac{1}{\lambda} \frac{1}{S(h_t)} \tag{3.24}$$

where λ is the *mean rate* defined as $\frac{N_t}{N_y}$, with N_t number of over-threshold events during the whole period analysed, and N_y number of years within the period; $S(h_t)$ is the tail function calculated in h_t. R is measured in years.
As regards hazard estimation, in each sea point the analysed period is 11 years and the tail function is calculated by (3.3) for Weibull fit of the *swh*-PDF. The return period of waves over a fixed h_t is obtained for each sea point and is multiplied by 365 (days), becoming daily indicator of wave-over-threshold presence. If R>1 it means R exceeds the day and no hazard is associated there. If the return period is within a day, the hazard is estimated:

$$H = 1 - [R(h_t) * 365]. \tag{3.25}$$

The result is an hazard map with values from 0 to 1 of increasing risk. In Fig. 3.10 an example is shown fixing $h_t = 3$ m for both regions studied.
Hopefully, future study will improve the trivial method suggested here.

Chapter 4

Conclusion

This study has investigated the probability distribution function of the significant wave height in Ionian Sea and Iberian Sea regions, during winter (January) and summer (July) period, using long-term (2007-2017) dataset from CMEMS hindcast product MEDSEA_HINDCAST _WAV_006_012. Weibull 2-parameters PDF provides a good fit for eleven-years SWH distribution but is not best descriptive of peak and tail. Besides, it does not fit well the more Gaussian-shaped distributions in the Atlantic Ocean. This limits are overcome using Exponentiated Weibull PDF for fitting.
Four parameters (mean, standard deviation, skewness, kurtosis), have been calculated for theoretical Weibull and Exponentiated Weibull PDFs and for observational *swh*-PDF in each sea point. As the relationship between kurt and skew and between skew and mean/std depend only on shape parameter k in Weibull case, kurt(skew) and skew(mean/std) plots have been used to find the agreement between observational data and a Weibull variable. It was found that Weibull fitness is very good but perfectible. Unluckily, this very method could not be applied to EW parameters, because of their dependence on the two shape parameters (α,k), which makes necessary a much larger dataset or a different ad hoc method. It is our hope that future study will find a method to compare Weibull and Exponentiated Weibull fitness.
To confirm Weibull PDF is a good approximation to the observational data, *swh*-PDFs have been fitted after cutting off the wave height seasonal part.
Finally, an hazard mapping method has been suggested, based on waves-over-threshold return period. After fixing a threshold height value beyond which waves are reputed dangerous for men overboard, we estimate the return period of over-threshold waves for each sea point. Lastly, we associate a risk value in range $[0 \div 1]$ to points with daily over-threshold waves presence. A sample hazard map has been shown for each region, referring to the January period. Considering the proposed method is trivial, future studies may improve employing wave breaking against boats.

Appendix A

Calculation of W and EW distribution parameters μ, σ, γ_1 and γ_2

Here we demonstrate how to calculate the four parameters of W and EW distribution (mean μ, standard deviation σ, skewness γ_1, kurtosis γ_2) starting from the formula of the z-th distribution moment:

$$E(x^z) = \int_0^\infty (x-\mu)^z f(x)\,dx, \qquad (z > 1) \tag{A.1}$$

where f(x) is the PDF and μ is the mean, the first moment, defined as:

$$\mu = \int_0^\infty x f(x)\,dx. \tag{A.2}$$

Starting from (A.1) and using (A.2) we can determinate the second moment, which is the square of the standard deviation:

$$\begin{aligned}\sigma^2 &= \int_0^\infty (x-\mu)^2 f(x)\,dx \\ &= \int_0^\infty x^2 f(x)\,dx + \mu^2 \int_0^\infty f(x)\,dx - 2\mu \int_0^\infty x f(x)\,dx \\ &= \int_0^\infty x^2 f(x)\,dx - \mu^2 \quad .\end{aligned} \tag{A.3}$$

In the same way we calculate the third and the fourth moments:

$$\begin{aligned}E(x^3) &= \int_0^\infty (x-\mu)^3 f(x)\,dx \\ &= \int_0^\infty x^3 f(x)\,dx - \mu^3 \int_0^\infty f(x)\,dx + 3\mu^2 \int_0^\infty x f(x)\,dx - 3\mu \int_0^\infty x^2 f(x)\,dx \\ &= \int_0^\infty x^3 f(x)\,dx - 3\mu\sigma^2 - \mu^3 \quad ,\end{aligned} \tag{A.4}$$

$$
\begin{aligned}
E(x^4) &= \int_0^\infty (x-\mu)^4 f(x)\,dx \\
&= \int_0^\infty x^4 f(x)\,dx - 4\mu^3 \int_0^\infty x f(x)\,dx + 6\mu^2 \int_0^\infty x^2 f(x)\,dx - 4\mu \int_0^\infty x^3 f(x)\,dx + \mu^4 \\
&= \int_0^\infty x^4 f(x)\,dx - 4E(x^3)\mu - 6\mu^2\sigma^2 - \mu^4 \quad . \qquad \text{(A.5)}
\end{aligned}
$$

By (A.3), (A.4) and (A.5) we obtain skewness and kurtosis values, defined as:

$$
\gamma_1 = \frac{E(x^3)}{\sigma^3}, \qquad \gamma_2 = \frac{E(x^4)}{\sigma^4}. \qquad \text{(A.6)}
$$

For W PDF (3.1), the mean value μ (A.2) becomes (3.11):

$$
\begin{aligned}
\mu_W &= \int_0^\infty x \frac{k}{\lambda}(\frac{x}{\lambda})^{k-1} \exp^{-(\frac{x}{\lambda})^k}\, dx \\
&= \lambda \int_0^\infty t^{(1+\frac{1}{k})-1} \exp^{-t}\, dt \\
&= \lambda\Gamma\Big(1+\frac{1}{k}\Big) \quad , \qquad \text{(A.7)}
\end{aligned}
$$

with change of variable t=$(\frac{x}{\lambda})^k$ between the first and the second line.
Seeing that the first term of each (A.3), (A.4), (A.5) for W PDF contributes as:

$$
\int_0^\infty x^z f(x)\,dx = \lambda^z \Gamma\Big(1+\frac{z}{k}\Big) \quad , \qquad \text{(A.8)}
$$

we use (A.3), (A.4), (A.5) and(A.6), obtaining (3.12),(3.13) and (3.14), as in Chu (2008 [10]).
For EW PDF (3.1), the mean value μ (A.2) becomes (3.15):

$$
\begin{aligned}
\mu_{EW} &= \int_0^\infty x\alpha \frac{k}{\lambda}(\frac{x}{\lambda})^{k-1} \exp^{-(\frac{x}{\lambda})^k}(1-\exp^{-(\frac{x}{\lambda})^k})^{\alpha-1}\, dx \\
&= \alpha\lambda \int_0^\infty t^{(1+\frac{1}{k})-1} \exp^{-t}(1-\exp^{-t})^{\alpha-1}\, dt \\
&= \lambda\Gamma\Big(1+\frac{1}{k}\Big)\sum_{i=0}^{\infty} \frac{(-1)^i}{(i+1)^{-(1+\frac{1}{k})}} P_{\alpha-i} \quad , \qquad \text{(A.9)}
\end{aligned}
$$

where

$$
P_{\alpha-i} = \alpha(\alpha-1)(\alpha-2)\cdots(\alpha-i).
$$

Between the first and the second line we used the change of variable t=$(\frac{x}{\lambda})^k$, while between the second and the third line the binomial expansion

$$
(1-x)^{\alpha-1} \approx 1-(\alpha-1)x+\frac{(\alpha-1)(\alpha-2)}{2!}x^2-\frac{(\alpha-1)(\alpha-2)(\alpha-3)}{3!}x^3+\cdots
$$

has been employed considering $\lim_{t\to\infty} \exp^{-t} = 0$.
Seeing that the first term of each (A.3), (A.4), (A.5) for EW PDF contributes as:

$$\int_0^\infty x^z f(x)\, dx = \lambda^z \Gamma\Big(1+\frac{z}{k}\Big) K(\alpha,k) \quad , \tag{A.10}$$

where:

$$K(\alpha,k) = \sum_{i=0}^{\infty} \frac{(-1)^i}{(i+1)^{-(1+\frac{1}{k})}} P_{\alpha-i} \quad ,$$

by (A.3), (A.4), (A.5) and(A.6), we obtain (3.16),(3.17) and (3.18), coherently with Pal's work (2006 [20]):

$$\sigma^2_{\mathrm{EW}} = \lambda^2 \left(\Gamma\Big(1+\frac{2}{k}\Big) - \Gamma^2\Big(1+\frac{1}{k}\Big) K(\alpha,k) \right) K(\alpha,k) \quad , \tag{A.11}$$

$$\gamma_{1\mathrm{EW}} = \frac{\Gamma\Big(1+\frac{3}{k}\Big) - 3\Gamma\Big(1+\frac{1}{k}\Big)\Gamma\Big(1+\frac{2}{k}\Big) K(\alpha,k) + 2\Gamma^3\Big(1+\frac{1}{k}\Big) K^2(\alpha,k)}{\Big[\Gamma\Big(1+\frac{2}{k}\Big) - \Gamma^2\Big(1+\frac{1}{k}\Big) K(\alpha,k)\Big]^{\frac{3}{2}} K^{\frac{1}{2}}(\alpha,k)} \quad , \tag{A.12}$$

$$\gamma_{2\mathrm{EW}} = \frac{\begin{array}{r}\Gamma\Big(1+\frac{4}{k}\Big) - 4\Gamma\Big(1+\frac{1}{k}\Big)\Gamma\Big(1+\frac{3}{k}\Big) K(\alpha,k) + \\ +6\Gamma^2\Big(1+\frac{1}{k}\Big)\Gamma\Big(1+\frac{2}{k}\Big) K^2(\alpha,k) - 3\Gamma^4\Big(1+\frac{1}{k}\Big) K^3(\alpha,k)\end{array}}{\Big[\Gamma\Big(1+\frac{2}{k}\Big) - \Gamma^2\Big(1+\frac{1}{k}\Big) K(\alpha,k)\Big]^2 K(\alpha,k)} \quad . \tag{A.13}$$

Bibliography

[1] Eisa Mahmoudi et al. " The Extended Exponentiated Weibull distribution and its applications". In: *STATISTICA, anno LXXVIII, n. 4* (2018).

[2] Hasselmann K. et al. "Measurements of wind-wave growth and swell decay during the Joint North Sea Wave Project (JONSWAP)". In: *Ergänzungsheft 8-12. Deutches Hydrographisches Institut* (1973).

[3] J.G. Komen et al. "Dynamics and modelling of ocean waves". In: *Cambridge University Press* (1994).

[4] Jaak Monbaliu et al. "The spectral wave model, WAM, adapted for applications with high spatial resolution". In: *Coastal Engineering* (2000).

[5] M. Ghil et al. "Extreme events: dynamics, statistics and prediction". In: *Nonlinear Processes in Geophysics, 18, 295–350* (2011).

[6] N. V. Teena et al. "Statistical analysis on extreme wave height". In: *Natural Hazards 64, 223–236* (2012).

[7] Snyder R.L. et al. "Array measurements of atmospheric pressure fluctuations above surface gravity waves". In: *J. Fluid Mech. 102, 1–59* (1981).

[8] Vladyslav Lyubartsev (Validator) et al. Anna Zacharioudaki. "QUID for MED MFC Products MEDSEA HINDCAST WAV 006 012". In: *CMEMS on-line documents* (2019). URL: `http://marine.copernicus.eu`.

[9] S. Straetmans C. Versluis. "Skewness Measures for the Weibull Distribution". In: *SSRN* (2015). URL: `http://dx.doi.org/10.2139/ssrn.2590356`.

[10] Peter C. Chu. "Probability distribution function of the upper equatorial Pacific current speeds". In: *Geophysical research letters, VOL. 35* (2008).

[11] Peter C. Chu. "Statistical Characteristics of the Global Surface Current Speeds Obtained From Satellite Altimetry and Scatterometer Data". In: *IEEE Journal of selected topics in applied Earth observations and remote sensing, Vol. 2, no. 1* (2009).

[12] A. Zacharioudaki et Al. G. Korres. "PRODUCT USER MANUAL For Mediterranean Sea Waves Hindcast Product MEDSEA HINDCAST WAV 006 012". In: *CMEMS on-line documents* (2019). URL: `http://marine.copernicus.eu`.

[13] Y. Goda. *Random seas and design of maritime structures*. Ed. by World Scientific Publishing Co. Pte. Ltd. Advanced Series on Ocean Engineering - Volume 15. 2000.

[14] WAMDI Group. "The WAM Model—A Third Generation Ocean Wave Prediction Model." In: *J. Phys. Oceanogr. 18, 1775–1810.* (1998).

[15] Behrens A. Günther H. "The WAM model. Validation document Version 4.5.4." In: *Intitute of Coastal Research Helmholtz-Zentrum Geesthach (HZG)* (2012).

[16] Hasselmann K. Hasselmann S. "Computations and Parameterizations of the Nonlinear Energy Transfer in a Gravity-Wave Spectrum. Part I: A New Method for Efficient Computations of the Exact Nonlinear Transfer Integral". In: *J. Phys. Oceanogr. 15, 1369–1977* (1985).

[17] Hasselmann K. et al. Hasselmann S. "Computations and Parameterizations of the Nonlinear Energy Transfer in a Gravity-Wave Specturm. Part II: Parameterizations of the Nonlinear Energy Transfer for Application in Wave Models". In: *J. Phys. Oceanogr. 15, 1378–1391* (1985).

[18] Y. Hu and R. T. Pierrehumbert. "The advection-diffusion problem for stratospheric flow. Part I: concentration probability distribution function." In: *J. Atmos. Sci. 58, 1493–1510* (2001).

[19] Hasselmann K. "On the spectral dissipation of ocean waves due to white capping. Boundary-Layer". In: *Meteorol. 6, 107–127* (1974).

[20] J. Woo M. Pal M.M. Ali. "Exponentiated Weibull distribution". In: *STATISTICA, anno LXVI, n. 2* (2006).

[21] Anna Zacharioudaki Michalis Ravdas and Gerasimos Korres. "Implementation and validation of a new operational wave forecasting system of the Mediterranean Monitoring and Forecasting Centre in the framework of the Copernicus Marine Environment Monitoring Service". In: *Natural Hazards and Earth System Science* (2018).

[22] N. Balakrishnan Norman L. Johnson Samuel Kotz. *Continuous Univariate Distributions*. second etition. Vol. 1. 1994.

[23] N. Balakrishnan Norman L. Johnson Samuel Kotz. *Continuous Univariate Distributions*. Vol. 2. 1995.

[24] Janssen P. "Quasi-linear Theory of Wind-Wave Generation Applied to Wave Forecasting". In: *J. Phys. Oceanogr. 21, 1631–1642* (1991).

[25] Janssen P. "Wave-Induced Stress and the Drag of Air Flow over Sea Waves". In: *J. Phys. Oceanogr. 19, 745–754* (1989).

[26] J.V. Seguro and T.W. Lambert. "Modern estimation of the parameters of the Weibull wind speed distribution for wind energy analysis". In: *Journal of Wind Engineering and Industrial Aerodynamics* 85.1 (2000), pp. 75–84.

[27] Navarra A. Sepp Neves A. A. Pinardi N. and F. Trotta. "A General Methodology for Beached Oil Spill Hazard Mapping". In: *Frontiers in Marine Science* 7 (2020), p. 65. URL: https://www.frontiersin.org/article/10.3389/fmars.2020.00065.

[28] K. Perera T. Thevasiyani. "Statistical analysis of extreme ocean waves in Galle, Sri Lanka". In: *weather and Climate Extremes 5-6, 40-47* (2014).

[29] H. Gildor Y. Ashkenazy. "On the Probability and Spatial Distribution of Ocean Surface Currents". In: *Journal of Physical Oceanography, Vol. 41* (2011).